Journal of Magnetism and Magnetic Materials 420 (2016) 204–209

Contents lists available at ScienceDirect

Journal of Magnetism and Magnetic Materials

journal homepage: www.elsevier.com/locate/jmmm

Comparison of microstructure and magnetic properties of 3% Si-steel, amorphous and nanostructure Finemet

M. Yousefi *, Kh. Rahmani, M.S. Amiri Kerahroodi

Energy and Mechanical Engineering Department, Power and Water College of Engineering, Shahid Beheshti University, P.O. Box.16765-1719, Tehran, Iran

ARTICLE INFO

Article history:
Received 15 January 2016
Received in revised form
24 June 2016
Accepted 11 July 2016
Available online 12 July 2016

Keywords:
Finemet
3%Si-steel
Microstructure and hysteresis

ABSTRACT

This paper presents a comparison of microstructure and magnetic properties of polycrystalline 3%Si-steel, amorphous and nano-crystalline alloy $Fe_{73.5}Cu_1Nb_3Si_{13.5}B_9$ (known as Finemet). Si-steels are industrially produced by casting, hot and cold rolling, annealing and coating. Samples of thin amorphous ribbons were prepared by the planar flow casting (PFC) method. Nano-crystalline samples are obtained after annealing in vacuum furnace at 560 °C for 1 h. The structure of specimens was investigated by XRD, SEM and FE-SEM. Also, magnetic properties were measured using vibrating sample magnetometer (VSM). The results showed that, hysteresis losses in as-quenched and nano-crystalline ribbons were by 94.75% and 96.06% less than 3%Si-steel, respectively. After the heat treatment of amorphous specimens, hysteresis area was decreased by 25% in comparison with heat treated specimen. This decreasing is occurred due to the formation of Fe_3Si nanostructure with size of 10–17 nm and removing segregation after heat treatment.

1. Introduction

One of the most important applications of soft magnetic materials is distribution and generator transformers cores. Si-steel containing 3% Si is one of the first magnetic materials, which was being used in production of transformer core sheets. This Steel has got the advantages including accessibility, cheapness and simplicity in production.

Due to the increase in global energy demand and absence of natural resources, energy saving has become a major concern in the last decades. Also, research and development of the magnetic materials is one way to solve part of the energy problems [1–4]. For this purpose, a new kind of material, Finemet, with amorphous and nano- crystalline structure has been developed in the last thirty years. Finemet alloy (Fe–Si–B–Nb–Cu) was introduced by Yoshizawa et al. in 1988 [4]. By rapid cooling of melt in Finemet alloy, an amorphous phase is created which is eligible to have a nanostructure with 10–20 nm grain size [1,4–9]. This amorphous system has recently attracted considerable interest due to its high magnetic permeability and saturation magnetization [1,10–12], which make it suitable for the transformer cores. Especially, this nano-crystalline material has also exhibited interesting magnetic properties under the appropriate heat treatment [1,13]. Alloys with nano grain size particles, in comparison with Si-steel ribbons and amorphous, could have very low hysteresis losses and high magnetic permeability [14]. The early transition metal Nb-atoms are stabilizers of the amorphous phase and are preferentially located at the periphery of crystal grains, which limit the grain growth and delay the B precipitation when the amorphous phase is under heat treatment. Cu-atoms are not soluble in Fe and serve as nucleating agent for the ferromagnetic nano-crystalline Fe–Si phase, favoring the nano-crystallization process [1,15–18].

Below the crystallization temperature, the internal stresses present in the as-quenched amorphous materials were relaxed, which can improve the magnetic responses. A subsequent heat treatment above its crystallization temperature produces an ultrafine structure of Fe–Si embedded in a disordered matrix. The crystallization mechanism follows a DO_3 structure of Fe_3Si type with a body-center-cubic phase (bcc) [1]. Main phase is Fe–Si and other section of structure, amorphous phase around crystalline grains of Fe–Si [5]. Alloys with this grain size, in comparison with Si-steel and amorphous have very low hysteresis losses and high magnetic permeability [14].

In this work, the as-quenched Finemet $Fe_{73.5}Cu_1Nb_3Si_{13.5}B_9$ ribbons were made via planar flow casting (PFC) method and then these ribbons were annealed. The effect of heat treatment and comparison with non-oriented 3%Si-steel ribbon was examined by using X-ray diffraction (XRD), scanning electron microscopy (SEM), field emission scanning electron microscopy (FE-SEM) and vibration sampling magnetometer (VSM). Moreover, this study examines both segregation and phase separation effect on Finemet magnetic properties.

* Corresponding author.
E-mail address: masoud_yousefi@hotmail.com (M. Yousefi).

http://dx.doi.org/10.1016/j.jmmm.2016.07.015
0304-8853/

2. Experimental procedures

Sheets of an ordinary distribution transformer core were used as 3%Si-steel sheets. Finemet alloy with the nominal composition of $Fe_{73.5}Cu_1Nb_3Si_{13.5}B_9$ was made by a planar flow casting (PFC) method, on a rotating metallic cylinder with 200 mm in diameter. The rate of cylinder rotation, equal to 2627 rpm, was corresponded to a linear surface velocity of 27.5 m/s., the wideness and the thickness of produced ribbons were 10 mm and 46 μm, respectively. The casting was performed by keeping the wheel-nozzle gap at 0.2 mm and ejection pressure at 78 kPa.

Amorphous ribbon samples were sealed in quartz tubes under technical vacuum (at 0.013 Pa pressure) and were isothermally annealed at 560 °C in the furnace atmosphere consisted of flowing protective Ar gas at 50 KPa pressure for 1 h and then 1 h cooling in the furnace. The annealing temperature for the ribbon was decided based on the crystallization temperature obtained from differential scanning calorimetric (DSC) by using non isothermal test (Netzsch, Germany) in the temperature range of 300–800 °C under Ar atmosphere at a constant heating rate of 20 °C/min.

The structural changes due to heat treatment of the amorphous samples and also the structure of 3%si-steel samples were investigated by X-ray diffraction (made by: Philips, Netherlands; model: PW3040/60). the X-ray diffraction patterns were obtained by using a diffractometer with CuKα radiation (45 kV/40 mA, $\lambda = 1.5406$ Å) with a nickel filter on the diffracted side. the scanning range was 30–120° (2θ) with a step size of 0.02°.

In order to evaluate and compare the magnetic properties of Finemet ribbons before and after heat treatment with 3%Si-steel Sheet, vibration sampling magnetometer (VSM) at 25 Hz frequency was used. Results of magnetic experiment were analyzed by the Origin 5.0 software.

Microstructural studies of the ribbons were performed by scanning electron microscope (Made by: TESCAN, Czech; Model: VEGA LMV) for 3%Si-steel Sheet and field emission scanning electron microscopy (Made by: TESCAN, Czech; Model: Mira 3-XMU) in the case of amorphous ribbons. Ribbons were investigated in the terms of phase separation and alloying elements distribution. Specimens were prepared by polishing, and then were etched 10 s by 2% nital solution.

3. Results and discussion

3.1. Microstructural studies

Fig. 1 shows 3%Si-steel sheet XRD's diffractions. Peaks were observed in 45°, 65°, 83°, 99° and 120° angels, peaks illustrate existence of ferrite phase in specimen microstructure and solid solution between Si and Fe atoms.

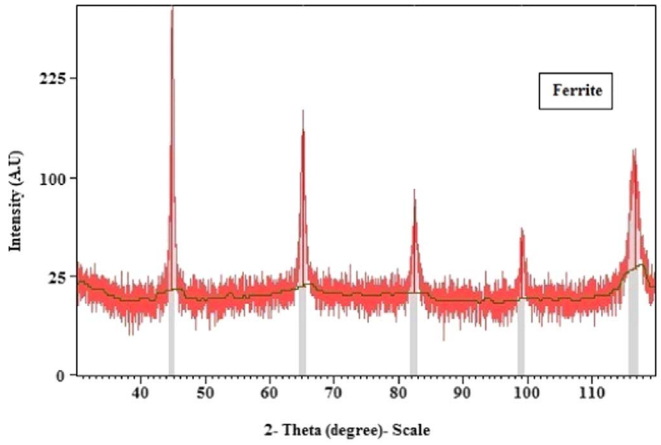

Fig. 1. XRD diffraction of 3%Si-steel specimen.

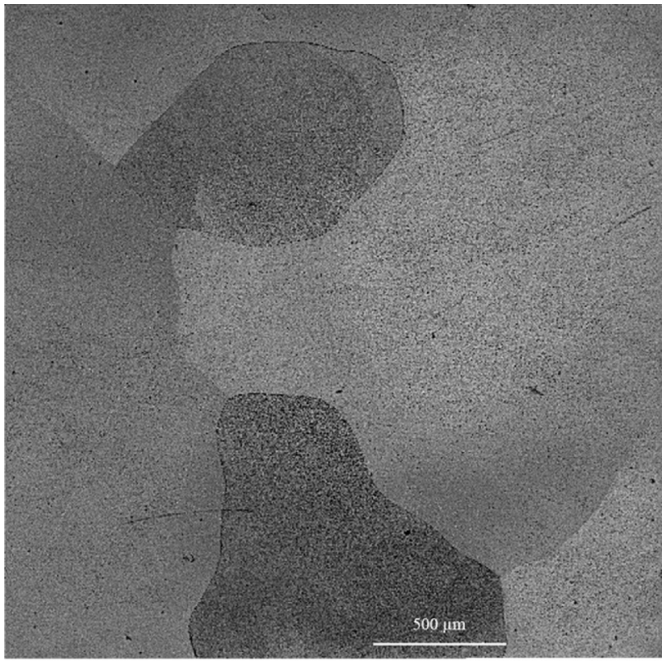

Fig. 2. SEM image of 3%Si-steel sheet.

Fig. 2 displays the microstructure of 3%si-steel. As shown in Fig. 2, grains size is even more than 1000 μm. Fig. 2 indicates that 3%Si-steel is large grain size which leads to high hysteresis losses of this sheet. As 3%Si-steel is formed by large grains, have different domains in each grain and magnetic saturation occurs in higher rates [19]. Consequently hysteresis area increases. However, as seen in Fig. 3, no segregation is observed. Therefore, phase separation does not affect, unlike the presence of different magnetic domains in each grain, which increases the hysteresis losses.

Fig. 4 shows DSC results for the as-quenched Finemet alloy. The DSC profile (Fig. 4) of the as-quenched Finemet alloy displays two main and highly intensive exothermic peaks with peak temperatures at 546 and 688 °C, respectively. The two intense peaks correspond to the two steps of crystallization. It has been reported that the crystallization of pure Finemet alloys takes place in two steps: the α-Fe (Si) primary and the FeB secondary crystallizations [1,20,21]. Consequently Annealing process was performed at 560 °C to avoid formation of boron compounds. It must be noticed that secondary stage of nano-crystallization occurs in higher temperatures and undesirable magnetic phases the same as Fe_3B, $Fe_{23}B_6$ and Fe_2B coexist inside of α-Fe(Si) crystals with larger grain size than before [1,3].

Fig. 5 displays the XRD patterns of the Finemet $Fe_{73.5}Cu_1Nb_3Si_{13.5}B_9$ alloy before and after isothermal annealing for 1 h at 560 °C temperature, which yields the effect of annealing on new phase formation. The XRD patterns of as-quenched Finemet alloy in Fig. 5(a) shows an amorphous phase only, with a broad diffraction peak 2θ at ~44°. The presence of halos definitely indicates that the amorphous state is formed during quenching. XRD analysis confirmed that after annealing as shown in Fig. 5(b), a body-centered cubic (bcc) phase was observed with diffraction angles 2θ at ~45°, 66° and 83° corresponding to partial α-Fe(Si) ferromagnetic phase with Fe_3Si structure surrounded by amorphous background [1,22].

Scherrer's procedure was used to estimate the size of particles.

$$t = \frac{k\lambda}{\beta \cos\theta} \quad (1)$$

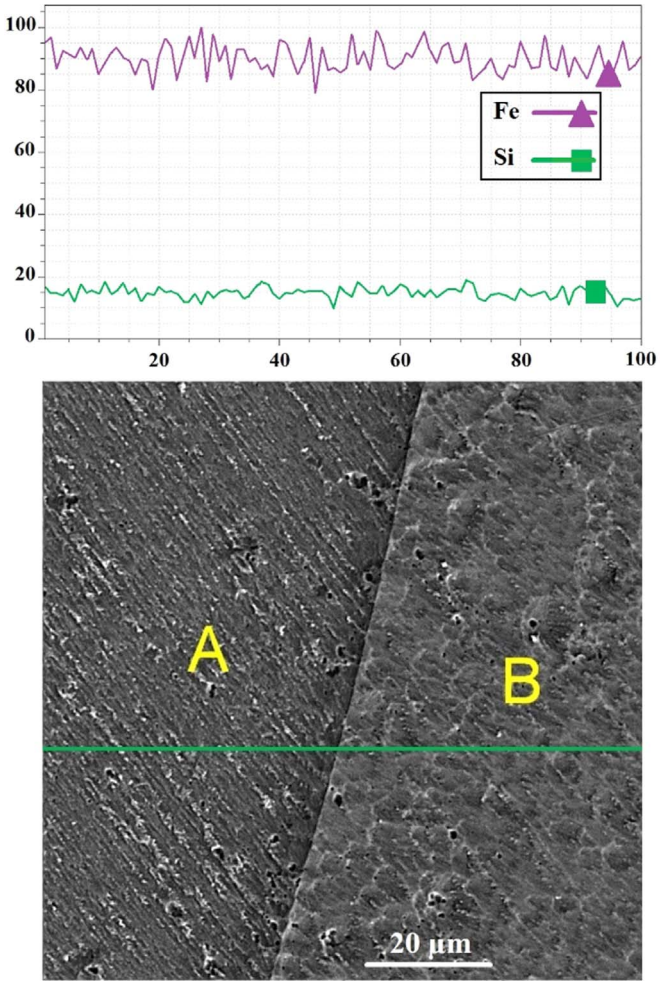

Fig. 3. SEM image of 3%Si-steel and linear scan analysis in grain boundary.

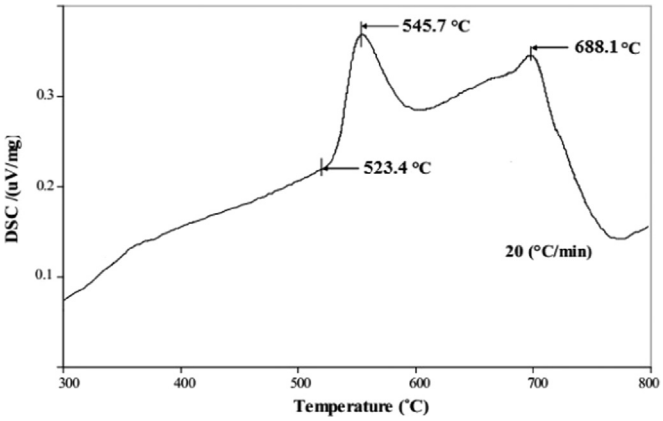

Fig. 4. DSC curve of as-quenched Finemet $Fe_{73.5}Cu_1Nb_3Si_{13.5}B_9$ alloy.

According to Scherrer's Eq. (1) [23], where t is average particle size (mm), K is crystal form factor (nearly is considered about 0/9), λ is wave length arising from X-ray tube (nm), β is pick width in half of maximum height (FWHM) and θ is diffraction angle in degree. The intensity of the X-ray diffraction pattern increases, indicating the crystallization of amorphous phase, and the crystalline grain size was estimated from the peaks of α-Fe(Si) phase to be about 10 to 17 nm. As shown in Fig. 5(b), lowering the broadened of halo is related to decreasing amorphous area, due to phase separation of α-Fe(Si) phase from amorphous background.

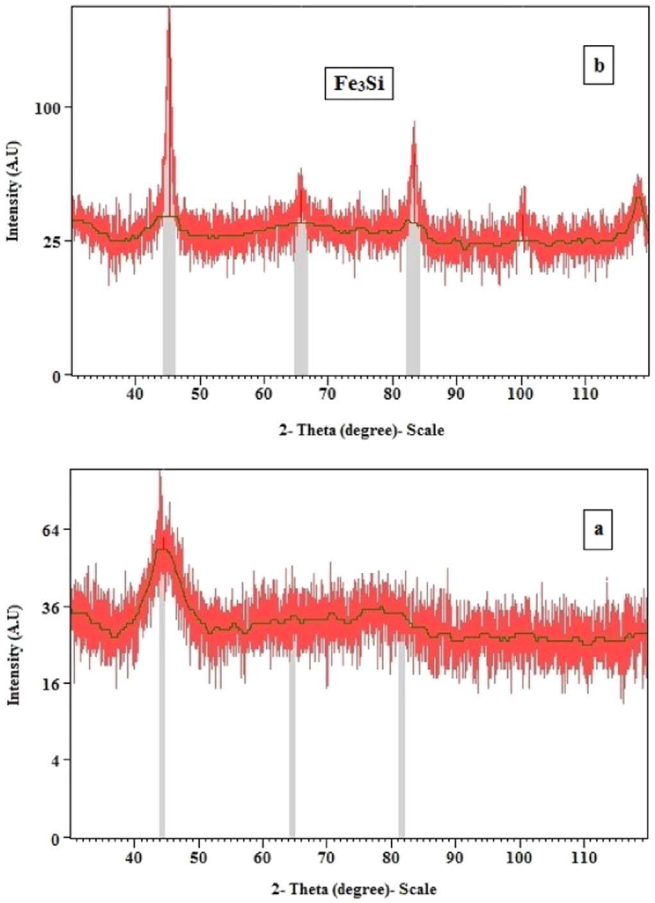

Fig. 5. XRD patterns of as-quenched and annealed Finemet alloy respectively in Fig. 5(a) and (b).

Fig. 6 displays FESEM image of Finemet alloy produced via PFC method and linear analysis of specific region in which color changes from gray to black. Linear scan analysis of in Fig. 6 shows that as-quenched specimen is not completely homogenous, chemical composition changes in some regions. There are two sharp picks corresponding to B and Fe elements, hence distribution of these two elements is not uniform. Whereas, high speed casting is under non equilibrium solidification condition, the segregation phenomenon occurs in some regions. This change in B content is totally different from phase separation due to formation of nano metric Fe_3Si, because it takes place in larger scale (about 200 μm). Moreover, the cluster formation effect creates a diffusion barrier due to the segregation of the refractory elements such as B atoms, which are responsible for the inhibition of iron-silicate grain growth [24]. Linear analysis in Fig. 7, confirms specimen homogeneity in comparison with as-quenched specimen. Changes in B content distribution cause localize defect because amorphous alloys needs to have the lowest possible B and Si contents, in order to guarantee good magnetic properties [25]. Therefore, high level of B in some regions is not remarkable.

3.2. Magnetic analysis

One of the major parameter in quality of produced ribbons is the percentage of the hysteresis losses. The inner area of B–H loop characterizes hysteresis losses. Fig. 8 shows hysteresis diagram of 3%Si-steel. Also, B–H loop diagram of as-quenched and annealed Finemet alloy is respectively illustrated in Fig. 9 ((a) and (b)). Table 1 summarizes our present study of the coercivity, H_c, in the whole range of structural correlation lengths starting from atomic

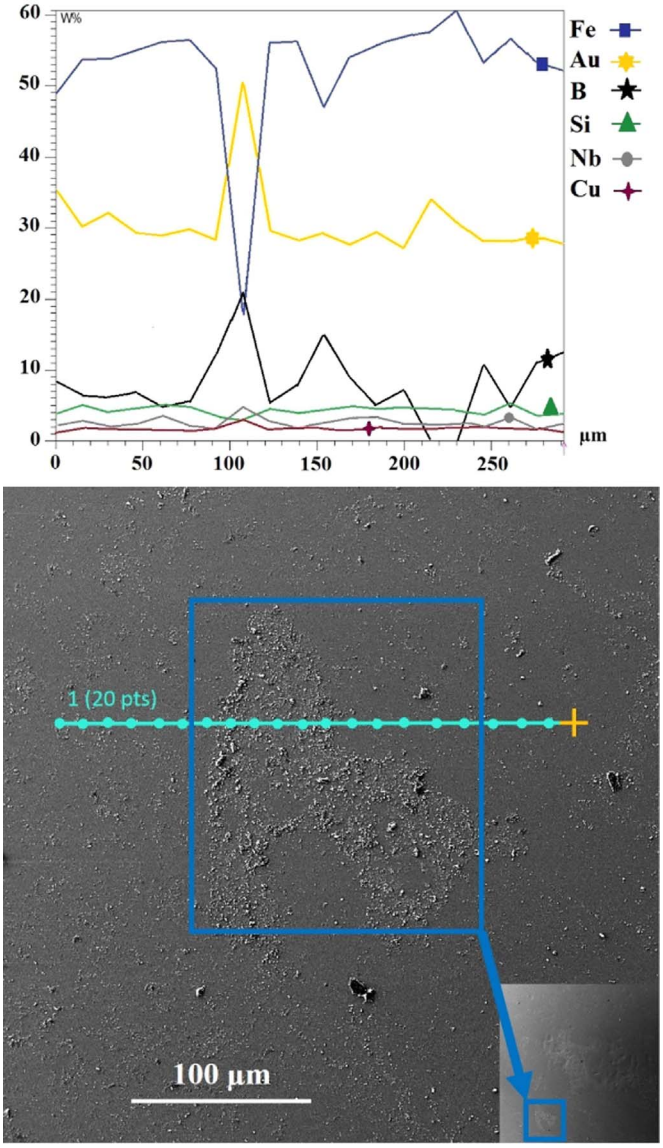

Fig. 6. FESEM image of as-quenched Finemet alloy specimen with linear scan analysis.

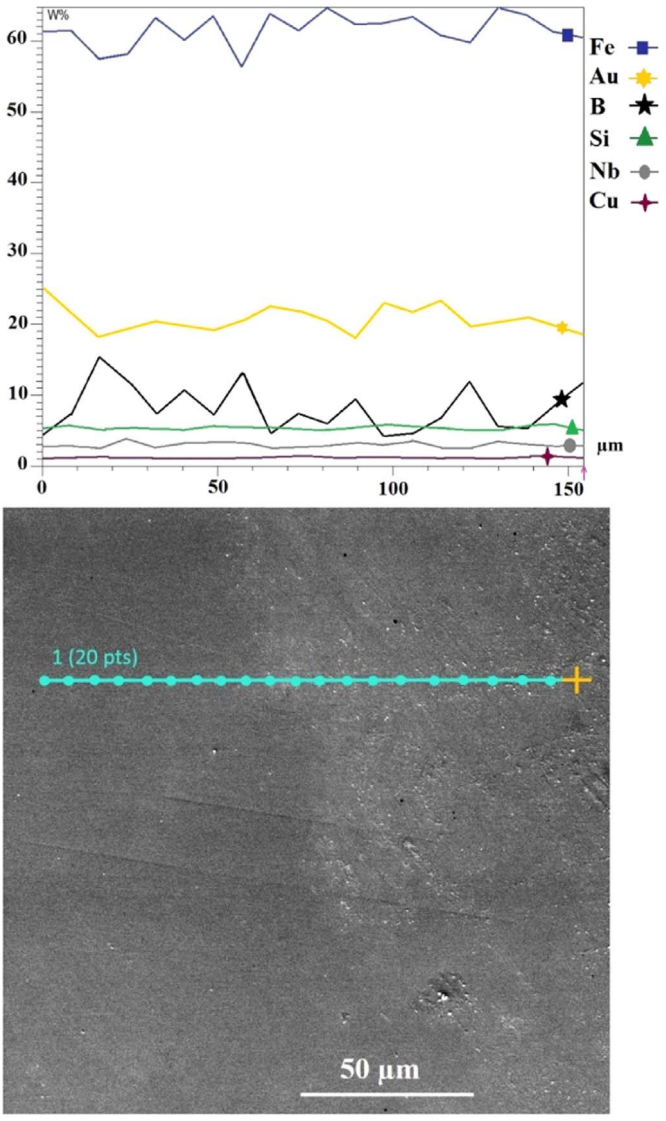

Fig. 7. FESEM image of annealed Finemet alloy specimen with linear scan analysis.

distances in amorphous Finemet alloy and nanometer regime up to macroscopic grain sizes in 3%Si-steel. Lower coercive force H_c leads to high permeability and low hysteresis losses. Magnetic parameters of as-quenched and ribbons were accordance with other research in the case of Finemet alloy [26,27].

Loss minimization is a very important area of concern in electricity transmission and even in distribution [28]. As illustrated in Table 1, there is a remarkable difference between the magnetic properties of as-quenched and annealed Finemet alloy along with 3%Si-steel. Finemet alloy after heat treatment has special properties such as: (1) Satisfy both high saturation magnetic flux density and high permeability (2) Low core loss (3) Low magnetostriction (4) Excellent temperature characteristics and small aging effects (5) Excellent high frequency characteristics (6) Flexibility to control magnetic properties "B–H curve shape" during annealing [5], which persuade power industry to replace the nanostructure materials (or amorphous) with 3%Si-steel. As shown in Table 1, after heat treatment of Finemet alloy, hysteresis area was decreased by 25% in comparison with as-quenched sample. As the external magnetic field varies at a *very low rate* periodically, due to the effects of magnetic domain wall motion the B–H relationship is

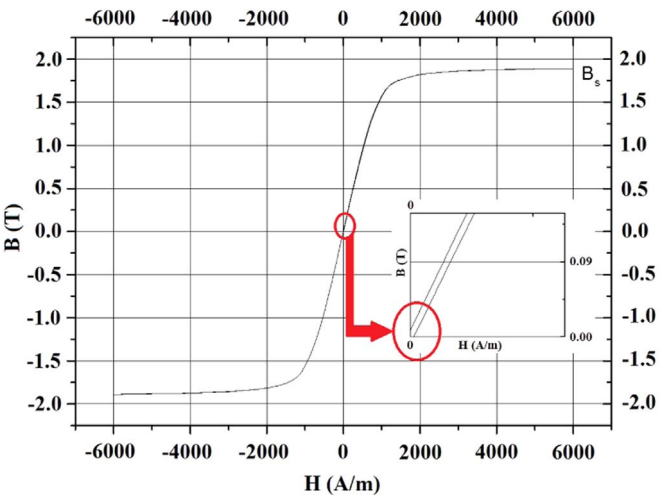

Fig. 8. B–H loop diagram of 3%Si-steel sheet.

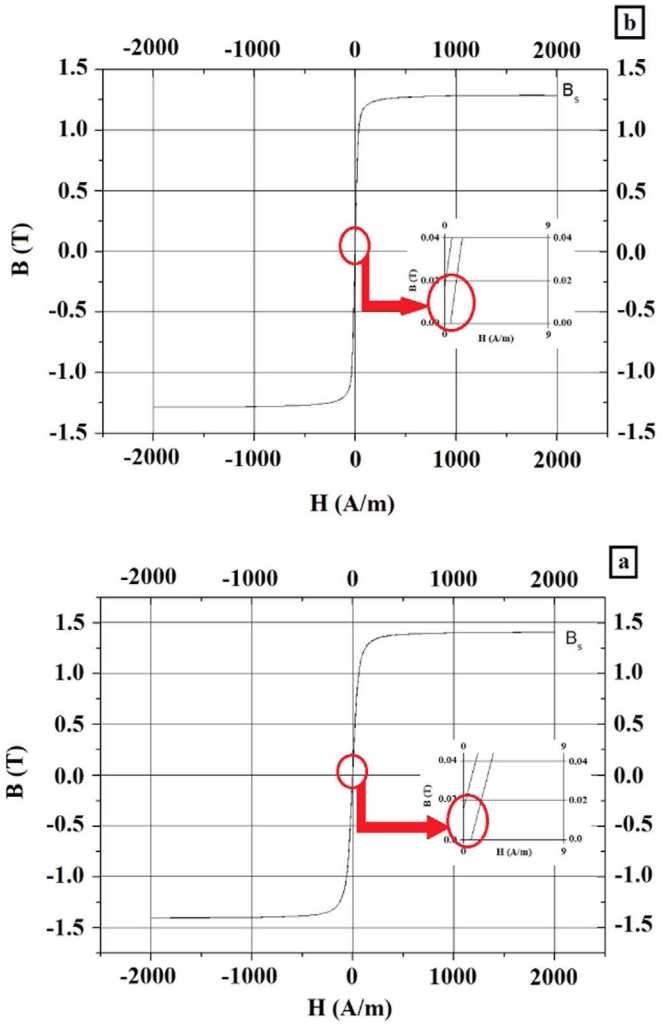

Fig. 9. B–H loop diagram of as-quenched (a) and annealed (b) Finemet alloy.

a hysteresis loop. The area enclosed by the loop is a power loss known as the hysteresis loss, and can be calculated by Eq. (2) [29]:

$$P_{hyst} = \oint H \bullet dB(W/m^3/cycle) \text{ or } (J/m^3) \quad (2)$$

where magnetic field strength (H), measured in amperes per meter (A/m), and magnetic flux density (B), measured in Newton-meters per ampere (N m/A), also called tesla (T). As it is shown in Figs. 8 and 9, although the B–H diagrams seem to be single line, as shown with higher magnification in red circles, there are two lines. By using origin software (version 5.0), it is possible to calculate the hysteresis area. As shown in Table 1, by comparing results of hysteresis area it was found out that the hysteresis area was reduced by 25%. Also, this calculation, can be used to comparison casted and annealed samples with 3%Si-steel. Based on hysteresis area of ribbons, if as-quenched amorphous ribbon is to be used instead of 3%Si-steel sheet, Hysteresis losses would be decreased by 94.75%, and by 96.06% with using annealed ribbon with nano metric particles of Fe_3Si in amorphous background. There are five factors for this reduction:(1) the Finemet alloy after heat treatment, was produced by crystallization of an amorphous Fe–Si–B alloy with small addition of Cu and Nb, unusual combination which proved to be key for the particular ultrafine grain structure and the associated soft magnetic properties. The particular about the material was it ultrafine microstructure of b.c.c Fe_3Si phase with grain size of 10–15 nm from which their soft properties lastly derive [30]. (2) It is well known that the microstructure, noticeably the grain size, essentially determines the hysteresis loop of a ferromagnetic material. The $1/D$-dependence of coercivity for large grain sizes reflects the conventional rule that good soft magnetic properties require very large grains ($D > 100\ \mu m$). Thus, the reduction of particle size to the regime of the domain wall width increases the coercivity Hc towards a maximum controlled by the anisotropies present. Lowest coercivities, however, are again found for smallest structural correlation lengths like in amorphous alloys ("grain size" of the order atomic distance) and in nano- crystalline alloys for grain sizes $D < 20$ nm. Obviously, Finemet alloy after heat treatment fills in the gap between amorphous metals and conventional poly-crystalline alloys (3%Si-steel) [30]. (3) Heat treatment of amorphous samples, let samples to release their stresses because of high speed casting. Also, the initial magnetic softening is produced by the relaxation of internal stresses (magnetoelastic anisotropy) within the amorphous state [31]. (4) Elimination of segregation after heat treatment or revision of B distribution without formation of harmful (Fe–B) crystalline parts. (5) Phase separation and formation of ferromagnetic Fe_3Si phase with proper nano metric dimensions as a result of selecting appropriate annealing time and temperature.

4. Conclusion

1. Before heat treatment, specimens produced via PFC method were completely amorphous and after heat treatment, nano metric phases of Fe_3Si were created and segregation was eliminated.
2. After heat treatment of amorphous sample, hysteresis losses decreased by 25%. Hysteresis losses of amorphous ribbon, was 94.75% less than 3%Si-steel and after heat treatment by formation of Fe_3Si, hysteresis losses was less than the 3%Si-steel sample by 96.06%. Consequently hysteresis losses of transformer cores can be considerably decreased.
3. In 3%Si-steel sheet, there are grains with more than 1000 μm dimension, no phase separation was observed and specimens were approximately homogenous. Therefore, hysteresis losses were only the result of different magnetic domains in each grain.
4. The main reason of low hysteresis losses in amorphous and nano ribbons is absence of different domains together which is arising from lack of crystalline structure grading in this material.
5. Replacement of 3%Si-steel with amorphous ribbons and annealed ribbons is quiet logical, because hysteresis losses decreases more than 90%.

Table 1
Magnetic parameters of as-quenched and annealed Finemet in comparison with 3%Si-steel sheet examined by VSM test.

Ribbon name	Hysteresis area	μ	B_s (Tesla)	$+H_c$ (meter/Amper)	$-H_c$ (meter/Amper)	$+B_r$ (Tesla)	$-B_r$ (Tesla)
As quenched Finemet	19.52	0.0127	1.4	0.61	0.69	0.015	0.016
Annealed Finemet	14.62	0.036	1.28	0.62	0.62	0.016	0.017
3% Si-steel	371.43	0.002	1.89	4.5	3.33	0.007	0.016

References

[1] M. Sorescu, T. Xu, S. Herchko, Recoilless fraction, structural, magnetic and thermal properties of $Fe_{73.5}Cu_1Nb_3Si_{13.5}B_9$ alloy, J. Magn. Magn. Mater. 323 (2011) 2859–2865.

[2] F. Marechal, D. Favrat, E. Jochem, Energy in the perspective of the sustainable development: the 2000 W society challenge, Resour. Conserv. Recycl 44 (2005) 245–262.

[3] J.M. Silveyra, E. Illeková, P. Švec, D. Janičkovič, A. Rosales-Rivera, V. J. Cremaschi, Phase transformation in Mo-doped FINEMETs, Phys. B. Condens. Matter 405 (2010) 2720–2725.

[4] Y. Yoshizawa, S. Oguma, K. Yamauchi, New Fe based soft magnetic alloys composed of ultrafine grain structure, J. Appl. Phys. 64 (1988) 6044–6046.

[5] Hitachi Metals, Ltd, Nanocrystalline soft magnetic material FINEMET, 2007, Brochure No. HL-FM10-D.

[6] A. Gavrilović, L.D. Rafailović, D.M. Minić, J. Wosik, P. Angerer, D.M. Minić, Influence of thermal treatment on structure development and mechanical properties of amorphous $Fe_{73.5}Cu_1Nb_3Si_{15.5}B_7$ ribbon, J. Alloy. Compd. 5095 (2011) S119–S122.

[7] X.Y. Zhang, J.W. Zhang, R.P. Liu, J.H. Zhao, Y.Z. Zheng, Influence of annealing temperature on the microstructure and initial permeability of the nanocrystalline alloy $Fe_{73.5}Cu_1W_3Si_{13.5}B_9$, J. Magn. Magn. Mater. 172 (1997) 301–307.

[8] G. Pozo López, L.M. Fabietti, A.M. Condó, S.E. Urreta, Microstructure and soft magnetic properties of Finemet-type ribbons obtained by twin-roller melt-spinning, J. Magn. Magn. Mater. 322 (2010) 3088–3093.

[9] K. Hono, D.H. Ping, Atom probe studies of nanocrystallization of amorphous alloys, J. Mater. Charact. 44 (2000) 203–217.

[10] G. Herzer, Grain size dependence of coercivity and permeability in nanocrystalline ferromagnets, IEEE Trans. Magn. 26 (1990) 1397–1402.

[11] M. Milglierini, J.M. Greneche, Mössbauer spectrometry of Fe(Cu)MB-type nanocrystalline alloys: I. The fitting model for the Mössbauer spectra, J. Phys. Condens. Matter 9 (1997) 2303–2319.

[12] K. Suzuki, Nanocrystalline soft magnetic materials: a decade of alloy development, Mater. Sci. Forum 312–314 (1999) 521–530.

[13] J. González, N. Murillo, J.M. Blanco, J.M. González, T. Kulik, Stress annealing in $Fe_{73.5}Cu_1Ta_3Si_{13.5}B_9$ amorphous alloy: induced magnetic anisotropy and variation of the magnetostriction constant, J. Appl. Phys. 76 (1994) 1131–1134.

[14] M.E. McHenry, M.A. Willard, D.E. Laughlin, Amorphous and nanocrystalline materials for applications as soft magnets, J. Prog. Mater. Sci. 44 (1999) 291–433.

[15] N. Kataoka, A. Inoue, T. Masumoto, Y. Yoshizawa, K. Yamauchi, Effect of additional Cu element on structure and crystallization behavior of amorphous Fe–Nb–Si–B alloys, J. Appl. Phys. 28 (1989) 1820–1823.

[16] M. Fujinami, Y. Hashiguchi, T. Yamamoto, Crystalline transformations in amorphous $Fe_{73.5}Cu_1Nb_3Si_{16.5}B_6$ alloy, J. Appl. Phys. 29 (1990) 477–480.

[17] M. Muller, N. Mattern, L. Illgen, The influence of different Cu/Nb contents on the structure and on the magnetic properties in nanocrystalline FeBSi base alloys, J. Magn. Magn. Mater. 112 (1992) 263–268.

[18] M. Sakurai, M. Matsuura, S.H. Kim, Y. Yoshizawa, K. Yamauchi, K. Suzuki, A fluorescence X-ray absorption fine structure study of the effect of small amounts of additives on the formation of the nanocrystalline phase from metallic glass, Mater. Sci. Eng. 179–180 (1994) 469–472.

[19] B.S. Mitchell, An Introduction to Materials Engineering and Sciences: For Chemical and Materials Engineers, John Wiley and Sons Inc., Hoboken , New Jersey , USA, 2004.

[20] F. Shahri, A. Beitollahi, S.G. Shabestari, S. Kamali, Effects of heat on the structural and magnetic properties of Al–Ge added $Fe_{73.5-x}Si_{13.5}B_9Nb_3Cu$ alloys, Phys. Rev. B. 76 (2007), 024434-1-13.

[21] P. Gorria, V.M. Prida, M. Tejedor, B. Hernando, M.L. Sánchez, Correlation between structure, magnetic properties and MI effect during the nanocrystallisation process of FINEMET type alloys, Phys. B. Condens. Matter 299 (2001) 215–224.

[22] E. Pulido, I. Navarro, A. Hernando, Mossbauer spectroscopy in nanocrystalline materials, IEEE Trans. Magn. 28 (1992) 2424–2426.

[23] A. Monshi, M.R. Foroughi, M.R. Monshi, Modified Scherrer equation to estimate more accurately nano-crystallite size using XRD, World J Nano Sci. Eng. 2 (2012) 154–160.

[24] V.A. Peña Rodriguez, J. Flores Regalado, E. Baggio-Saitovitch, E.C. Passamani, Nanocrystallization process in Finemet-type alloys followed by in situ 57Fe Mössbauer spectroscopy, J. Alloy. Compd. 379 (2004) 23–27.

[25] G. Shao, B. Lu, Y.Q. Liu, P. Tsakiropoulos, Glass forming ability of multi-component metallic systems, Intermetallics 13 (2005) 409–414.

[26] G.T. Nikolov, V.C. Vachev, Nanocrystalline magnetic materials versus ferrites in power electronics, Proc. Earth Plan. Sci. 1 (2009) 1357–1361.

[27] M. Hasiak, M. Lukiewski, M. Miglierini, J. Kaleta, Investigation and application of nanoperm- type soft magnetic materials, Acta Phys Polo. A 118 (2010) 829–831.

[28] O.M. Bamigbola, M.M. Ali, M.O. Oke, Mathematical modeling of electric power flow and the minimization of power losses on transmission lines, Appl. Math. Comp. 241 (2014) 214–221.

[29] G. Bertotti, Hysteresis in Magnetism:for Physicists, Materials Scientists, and Engineers, Academic Press, San Diego , California , USA, 1998.

[30] G. Herzer, "Chapter 3 Nanocrystalline soft magnetic alloys", Handbook of Magnetic Materials. 10, 1997, pp. 415–462.

[31] L. Sabetinejad, N. Sabetinejad, G. Kheiry, Nanocrystallization process in soft magnetic nanocrystalline alloy $Fe_{73.5}Si_{13.5}B_9Nb_3Cu_1$ studied by Mössbauer spectroscopy, Int. J. Res. Chem. Meta Civ. Eng. 2 (2015) 83–86.